Earth's field MRI for the non-invasive detection of fouling in spiral-wound membrane modules in pressure vessels during operation

R. Ujihara[a], E.O. Fridjonsson[a,*], N.W. Bristow[a], S.J. Vogt[a], S.S. Bucs[b], J.S. Vrouwenvelder[b,c], M.L. Johns[a]

[a]Department of Chemical Engineering, The University of Western Australia, Crawley WA 6009, Australia,
email: 20928627@student.uwa.edu.au (R. Ujihara), einar.fridjonsson@uwa.edu.au (E.O. Fridjonsson),
21700872@student.uwa.edu.au (N.W. Bristow), sarah.vogt@uwa.edu.au (S.J. Vogt), michael.johns@uwa.edu.au(M.L. Johns)
[b]Biological and Environmental Sciences and Engineering Division, Water Desalination and Reuse Center, King Abdullah University of Science and Technology, Thuwal 23955-6900, Saudi Arabia, email: szilard.bucs@kaust.edu.sa (S.S. Bucs),
johannes.vrouwenvelder@kaust.edu.au (J.S. Vrouwenvelder)
[c]Department of Biotechnology, Faculty of Applied Sciences, Delft University of Technology, Van der Maasweg 9, 2629 HZ Delft, The Netherlands, email: j.s.vrouwenvelder@tudelft.nl (J.S. Vrouwenvelder)

ABSTRACT

Fouling of spiral-wound reverse osmosis (SWRO) membrane systems is a pervasive problem. Here we demonstrate that a mobile, low cost magnetic resonance imaging (MRI) apparatus operating at the earth's magnetic field (low magnetic field, LF) can non-invasively (i) image the inside of a SWRO membrane system with glass fiber outside casing in a pressure vessel during cross flow operation and can (ii) detect the location of foulant, in this study sodium alginate. LF-MRI images of the module were successfully acquired in less than eight minutes using a spin-echo protocol, the internal structure of the modules was clearly evident and images compared well with high resolution MRIs obtained using a large-sized, costly high magnetic field superconducting MRI system. By parameter optimisation (specifically the echo time employed) it was possible to differentiate flowing and stagnant fluid in the clean and fouled membrane systems, and to determine the presence of alginate foulant on the feed-side of the fouled SWRO membrane system. This study motivates further investigation of the sensitivity of LF-MRI and the development of bespoke low cost LF-MRI hardware for the monitoring of industrial SWRO membrane installations.

Keywords: SWRO; Spiral wound reverse osmosis; Nanofiltration; Fouling; MRI

1. Introduction

In many parts of the world, projected demand for freshwater exceeds availability due to increasing population and overuse of non-renewable sources. Seawater desalination and wastewater reuse provide additional capacity for potable, agricultural and industrial water production, and hence is regarded as a solution to overcome water shortages. Reverse osmosis (RO) membranes are globally used for desalination and wastewater reuse projects due to the high quality of produced water (monovalent salt rejection of 92–99.9%) [1]; RO technology accounts for approximately 50% of the world's desalination capacity [2], with demand expected to grow worldwide.

Stable production of water by RO requires careful control of membrane fouling [3,4], the accumulation of fouling material within the membrane system. This will impact hydrodynamic performance of the module and may manifest through increased feed channel pressure drop, reduced permeate production or increased salt passage. Among the different types of fouling, excess biofilm growth in the feed spacer channel (biofouling) is known to be difficult to eliminate as even with extensive pre-treatment (99.99% microbial

*Corresponding author.

removal) enough bacterial cells remain to grow within the membrane systems at the expense of biogradable nutrients in the feedwater [5]. Once a large part of the membrane is fouled, chemical cleaning is no-longer effective due to poor mixing between the narrow flow channels and stagnant regions [6]. For this reason an area of significant research interest is the development of an early warning system for biofouling [7].In this work alginate, a long chain polysaccharide, is used to simulate the physical properties of extracellular polymeric substances (EPS) which makes up the bulk of biofilm material [8]. There is significant precedent in the use of alginate as a substitute material in membrane biofouling studies and the conditions for alginate fouling are well defined [9–14] allowing systematic and reproducible study of biofouling inside SWRO membrane systems.

The current development of monitoring technologies outlined in this work aims to achieve more robust, reliable detection of biofouling than pressure drop and permeate flux monitoring. Current practice with respect to membrane operation initiates corrective actions when pressure drop increases by 15% over a whole installation (6–8 modules in series), this has been reported as being ineffective for the control of biofouling [7]. Vrouwenvelder et al. [9] found that the lead membrane experiences faster biofilm deposition than the downstream membranes, supporting indicative measurements of biofouling being performed on this lead module. Vrouwenvelder et al. [7] also thus developed a small membrane fouling simulator (MFS) to predict biofilm growth. Their results indicate that measurements on the MFS can achieve more sensitive detection of fouling than the measurement of water quality parameters such as adenosine triphosphate (ATP) concentration, total cell count and assimilable organic carbon (AOC) in the feed water [10]. Other promising sensor developments include the use of ultrasonic time domain reflectometry (UTDR) [11,12]. UTDR evaluates the thickness of deposit on membrane by measuring the reflected ultrasonic echo. Although it has been demonstrated to successfully detect fouling, the attenuation of the acoustic signal inhibits sensing of the inner part of membrane systems [11]. Amorphous and dynamic morphologies of biofilm and slight movement of membrane envelope also poses difficulty in the interpretation of the acquired signal [11,12]. There are a number of other sensors [15–17] and microscopy techniques [18,19] that have been used in the literature to detect and characterize biofouling in membrane systems. For further information on fouling monitoring techniques many reviews are also available [20–22]. Recent work on electrical impedance spectroscopy (EIS) has shown potential at determining the early onset of fouling [17] by applying alternating current via external electrical contacts, an alternative on previous EIS methods which required insertion of electrodes into the feed and permeate solution, however this approach required adjustment of the membrane surface by surface metal sputtering to enhance the conduction properties of the system.

Recently, low field nuclear magnetic resonance techniques have been applied for the early detection of biofouling in a spiral wound RO membrane system [23,24]. The use of low field NMR enables the use of a compact, portable apparatus compared with superconducting high magnetic field instruments, this however also reduces the achievable signal-to-noise ratio. In the current study the work by Fridjonsson et al. [23] is extended to enable spatially resolved imaging measurements via 2D low magnetic field MRI [25]. As such the aim is to determine the ability of this type of technology to detect the spatial distribution of fouling across the cross-section of the membrane system non-destructively and non-invasively during operation. This is motivated by the desire to implement low field (LF) MRI technology at the industrial scale where a high field (HF) MRI system using a superconducting magnet requiring cryogenic fluids is cost prohibitive and insufficiently robust. The next sections will show results obtained using the same flow loop and membrane systems obtained using a LF-MRI system and HF-MRI for comparison. The aim of this study is to demonstrate that the LF-MRI system can non-invasively (i) detect fouling in membrane system during operation, and (ii) give spatial information about the fouling which would enhance cleaning efficiency.

2. Materials and methods

2.1. Magnetic resonance imaging

The low magnetic field (earth's field) measurements were conducted usinga Terranova-MRI instrument (Magritek, New Zealand) controlled using Prospa (v3.24) software. This instrument uses an electromagnet (18.8 mT) to pre-polarize the sample before detecting the signal at the local earth's magnetic field (~51 μT) at a ^{1}H Larmor resonant frequency of ~2185 Hz. This signal was obtained almost exclusively from water molecules. Magnetic resonance imaging was conducted using a 2D spin-echo imaging sequence, as shown in Fig. 1, details of MRI experimental parameters used are listed in the figure caption. The image contrast was adjusted by varying the echo time (T_E) from 200 to 800 ms. This changes the interval between the excitation pulse (90° pulse) and the detection of the signal. For a stationary sample, due to spin-spin relaxation (T_2 relaxation), the signal amplitude decreases. During flowing measurements this effect is coupled with a washout effect over t_E as fluid leaves the detection volume. Note the imaging slice is perpendicular to the direction of fluid flow and the flush-out effect becomes more severe as T_E is increased [26]. This facilitates a relatively simple but robust contrast mechanism between stagnant and flowing fluid. The voxel amplitudes of each image were divided by the mean noise amplitude to produce a signal-to-noise ratio (SNR) map of each image (obtained from the non-membrane area of the image). Images were threshold-masked to remove noise signal from space between the pressure vessel and the outer membrane glass fiber casing.

In order to quantify the difference between the clean and fouled membranes, high resolution magnetic resonance images (MRIs) of the membrane were acquired using a Bruker Biospec 9.4 T MRI scanner (radiofrequency (RF) coil diameter: 154 mm, gradient strength 0.33 T/m). Multi slice multi echo (MSME) MRI pulse sequence was used to acquire images at different echo times in a single scan (15 to 450 ms with echo spacing 15 ms, resulting in 30 images). Read and phase directions were along the cross-section of the membrane system, and slice direction was along the flow direction. Images with 20 mm slice thickness were acquired, resulting in voxel resolutions of 0.1 mm by 0.1 mm by 20 mm. The voxel amplitudes were normalised by
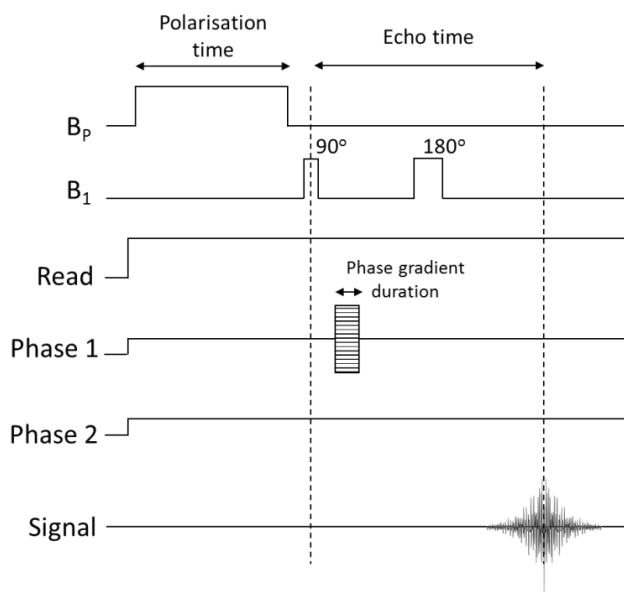
Fig. 1. Timing diagram for the 2D spin-echo imaging sequence for LF-MRI. B_p is the pre-polarisation field, B_1 is the applied radiofrequency coil field. Read & Phase 1 are the in-plane field (X, Y) and Phase 2 is the axial direction (Z). Note that these three gradients are also used for shimming purposes and thus the baseline for all three is not zero (as shown). For the measurements in this work polarisation time was 2000 ms, phase gradient duration was 50 ms, echo time was 200, 400 or 800 ms and a repetition time 4000 ms was used. Each scan was averaged four times and CYCLOPS [16] phase cycling was used. A sine-bell-squared filter was applied to the acquired signal. The bandwidth was set at 32 Hz, field of view (FOV) was 100 mm × 100 mm with an in-plane resolution 3.125 mm × 3.125 mm for a slice thickness of 170 mm (as determined by the B_1 length). The total 2D image acquisition time was 8 min 32 sec.

the mean voxel amplitude of water in the permeate tube. The images were threshold-masked to remove noise signal from space outside the membrane housing and between the housing and membrane, as well as the permeate channel.

2.2. Membrane system and flow setup

A spiral-wound RO membrane (XLE-2521, DOW FILM-TEC, USA) was used and contained within a fiberglass pressure vessel (total length 800 mm, outer diameter 75 mm, PV-2521-SW, HCTI, CA, USA); hereafter collectively referred to as the membrane system. The membrane system was inserted into the RF coil of the MRI instruments, and connected to a flow loop as shown in Fig. 2a. The inlet region of the membrane (6–23 cm from the front end of the membrane system) coincided with the axial length of the RF coils used and as such defined the volume from which NMR signal was received. Before imaging, the membrane was flushed in order to remove residual preservative chemicals as well as any air bubbles. This was applied exclusively to the feed channel side with the permeate channel being closed off. The process was applied for up to 12 h and only halted once no bubbles were observed to emerge

for a sustained period of time. The membrane and housing were placed in the RF coil, and connected to a flow loop (see Fig. 2a for detail). During the MRI scans, volumetric flow rate (Q) of feed water was maintained at 200 L/h (~5.7 cm/s average velocity on the feed side). The schematic of the structure of the membrane system is shown in Fig. 2b. Deionised water (conductivity < 1 μS/cm, Ibis Technology, WA, Australia) was used in all the experiments. Sodium alginate solution were prepared by dissolving 0.14 g/L of sodium alginate (Manugel® GMB alginate, IMCD Australia Ltd), 0.66 g/L of NaCl (99.7%, Chem-Supply-Australia) and 0.95 g/L of $CaCl_2$ (analytical reagent grade, Thermo Fisher Scientific-Australia) into the deionised water. Small dosages (25 ml) of alginate solution was introduced to the pump suction of a centrifugal pump for a total alginate loading of 130 mg. The system was then periodically flushed at 400 L/h with the permeate line isolated to dislodge any loose material in the system. During this process differential pressure (E&H PMP131-A2501Q4S 400) and membrane permeate and concentrate discharge flow rates (Stubbe DFM165: 5–60 L/h and DFM350 30–300 L/h respectively) were monitored.

2.3. Experimental procedures

During MRI image acquisition, the feed flow rate (Q) was fixed at 200 L/h. The MRI images were acquired using clean and fouled membranes to examine whether low magnetic field MRI can distinguish the different conditions of the membranes. MRI images of the clean membrane were acquired over a period of two months to monitor any changes in membrane system performance. The feed water was changed regularly; no increase of feed channel pressure drop was observed during this time indicating negligible system fouling. Then the feed solution in the reservoir was switched to a 0.14g/L sodium alginate solution and the operation of the membrane system observed over a period of two hours. The feed channel pressure drop before/after fouling is shown in Table 1. After the membrane was fouled, MRI images were taken with the feed solution changed back to deionised water. The feed channel pressure drop gradually increased from 26 kPa to 39 kPa over a period of two months due to rearrangement of fouling material and potentially some limited biological growth inside the membrane system, negligible permeate production was observed during the measurements.

3. Results and discussion

3.1. High magnetic field (400 MHz) MRI

Magnetic resonance images (MRIs) of the clean and fouled membrane systems at flowing conditions (Q: 200 L/h) at two different echo times (T_E: 30 ms and 90 ms) are shown in Fig. 3. The echo time corresponds to the time between volume excitation and detection, during which time fluid may wash-out of the RF coil causing signal attenuation. The clean membrane system shows a decrease in signal amplitude due to fluid wash-out effect as well as NMR relaxation as the echo time increases. When the clean and fouled membranes are compared there is an increase in spatial heterogeneity of signal distribution compared to the
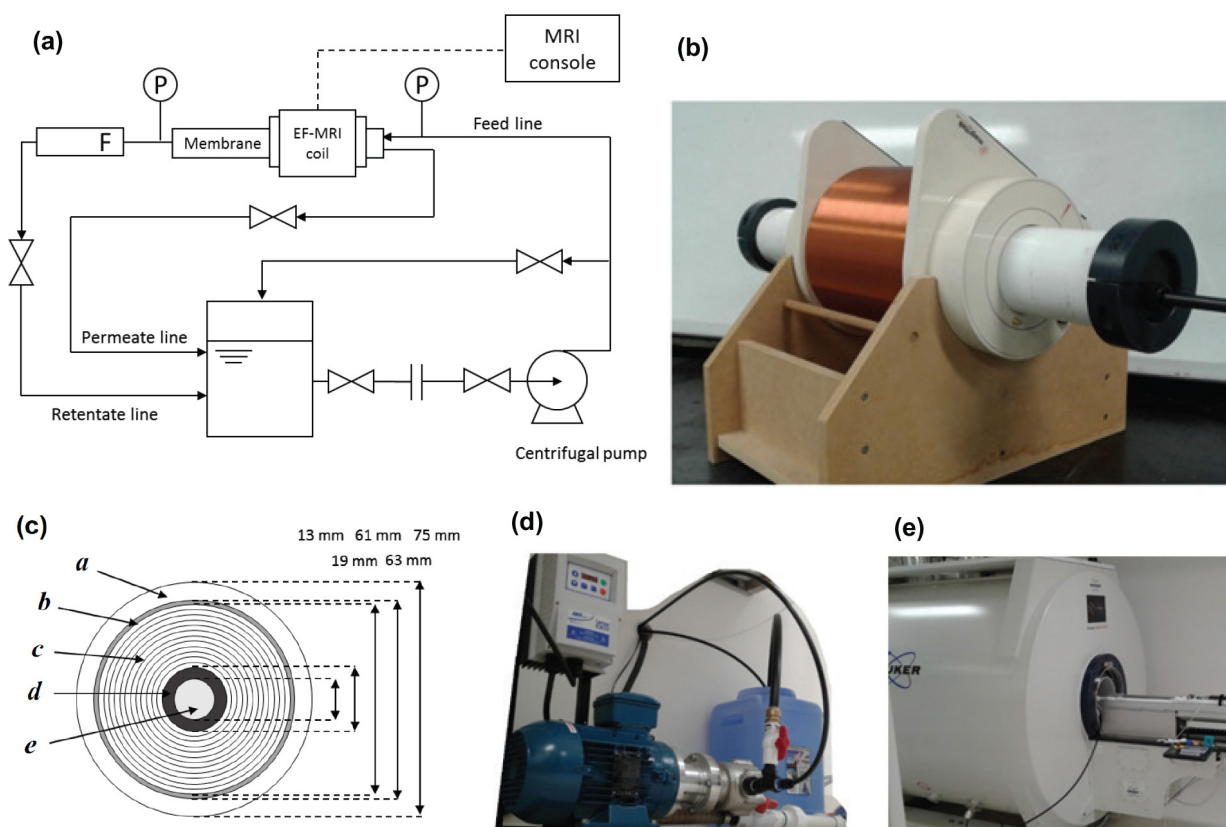
Fig. 2. Schematics and photographs of (a) membrane module flow loop; (b) membrane system inside low magnetic field MRI system; (c) spiral-wound membrane system cross section dimensions (*a*: wall of pressure vessel, *b*: opening between housing and membrane, *c*: membrane and spacer, *d*: wall of permeate tube, *e*: interior of permeate tube); (d) centrifugal pump with controller and tank; (e) membrane system inside high magnetic field MRI system.

clean membrane, with some feed channels with high normalised signal amplitude. These bright regions correspond to feed channel regions where fouling has caused fluid flow retardation and stagnation such that the wash-out effect is diminished. This formation of back-bone flow due to membrane fouling has been observed previously by Graf von der Schulenburg et al. [27] due to fouling increasing flow resistance in some feed spacer channels while other channels are either not fouled, or less fouled resulting in higher flow in those spacer regions. These images therefore demonstrate the effect of the sodium alginate gel on the flow distribution inside the membrane system, which results in a higher feed channel pressure drop across the membrane system as reported in Table 1.

While it is clear from Fig. 3 that a high field MRI system can easily distinguish between regions affected by fouling it is of significant practical interest to determine the sensitivity of a low-cost MRI platform such as an EF-MRI for the development of this technology for industrial applications.

3.2. Low magnetic field (earth's field) MRI

Low magnetic field (LF) MRI images, corresponding to the same system as was imaged in the HF-MRIs of clean and fouled membranes are shown in Fig. 4. For these images echo times of 200 ms and 800 ms are used to allow for sim-

Table 1
Feed channel pressure drop of the membrane at the flow rate (Q) of 200 L/h

	Clean	Fouled
Feed channel pressure drop (kPa)	5.3	26–39

ilar wash-out effect due to the larger slice thickness of 170 mm. For each of the operating conditions shown at least 39 MRI images were acquired to allow for statistical analysis of any transient environmental effects due to the low signal-to-noise ratio. The high signal amplitude at the center of the images is from the stationary water in the permeate tube (for contrast this has been masked out in the high field images). The signal from non-membrane area (noise) was removed using a signal threshold mask, and is not shown in the figure, the high signal intensity ring around the periphery of the membrane is due to water present between the pressure vessel and membrane element. The necessarily weaker gradients, the use of a more aggressive signal filter and the 1D (read direction) spectral broadening for low field MRI compared with high field MRI means there is a loss of image resolution and hence contrast, this causes for example the location corresponding to the wall of the per-
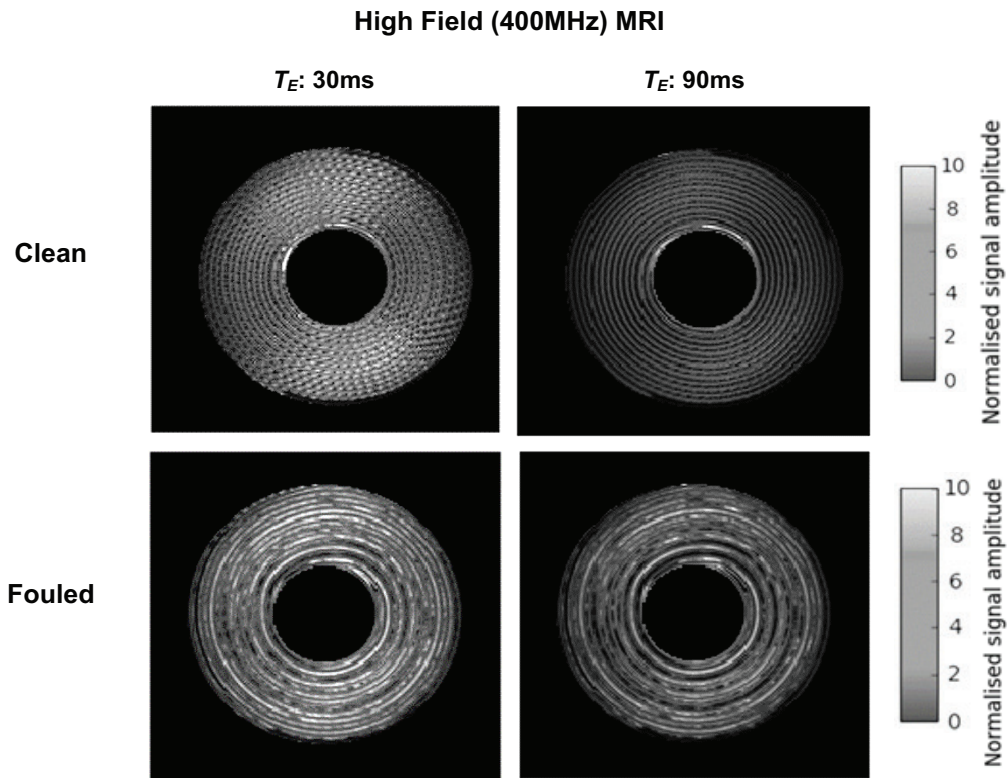
High Field (400MHz) MRI

Fig. 3. High resolution MRI images of clean and fouled membranes during cross-flow (Q: 200 L/h) measurements at echo times (T_E) of 30 and 90 ms. The decrease in signal intensity at different echo times is primarily due to wash-out effect. The increased heterogeneity in signal amplitude in the fouled membrane vs. clean membrane is due to increased heterogeneity of the flow field due to fluid stagnation and increased outflow in other regions. In-plane resolution: 0.1 by 0.1 mm, slice thickness: 20 mm.
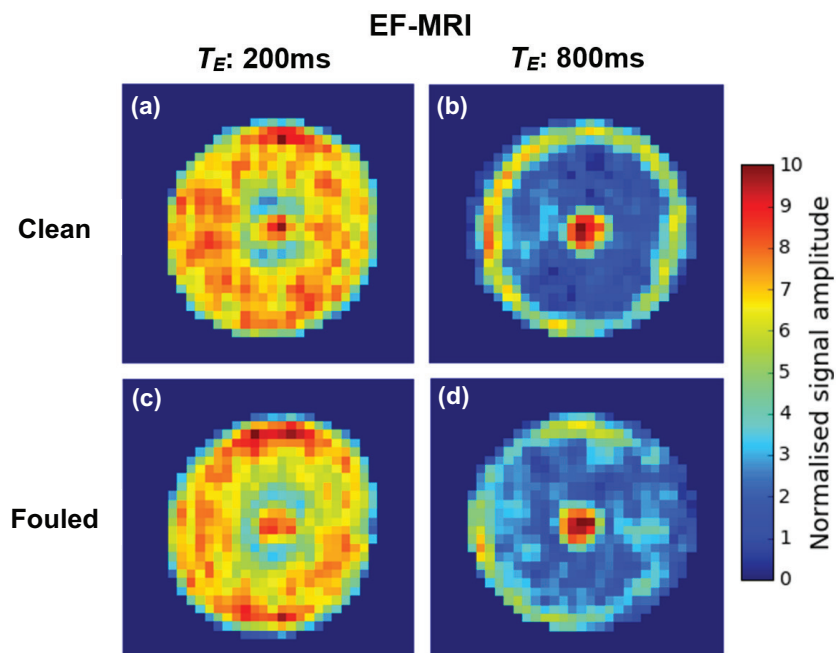
EF-MRI

Fig. 4. LF-MRI images acquired at Q: 200 L/h for clean membrane at (a) T_E: 200 ms and (c) T_E: 800 ms and fouled membrane at (b) T_E: 200 ms and (d) T_E: 800 ms. The membrane system in the clean and fouled cases are the same as those shown in Fig. 3. In-plane resolution: 3.125 mm by 3.125 mm, slice thickness 170 mm.

meate tube to apparently contain MRI signal due to signal contribution from neighboring voxels. Overall this causes a loss of voxel contrast at lower resolution compared with the HF-MRIs shown in Fig. 3. This means that simple masking of the permeate channel and water between membrane housing and membrane is not possible for the LF-MRIs and the choice of membrane analysis region must be done carefully to minimize the contribution of each of these regions to the signal in the membrane area (see Fig. 5 for reference).

When the clean and fouled membranes are compared with each other at different echo times (T_E: 200 ms and 800 ms) there is not much difference at the shorter echo time, while for the longer echo time the membrane region has more signal contrast between different regions. This is due to the effect of foulant build-up changing the fluid flow field within the membrane system, *e.g.* causing more stagnant fluid voxels resulting in higher signal amplitude. To investigate this apparent increase in heterogeneity of the signal amplitude, a comparison was done between the mean voxel amplitude of the feed side region at flowing (Q: 200 L/h) and non-flowing (Q: 0 L/h) conditions for the fouled and non-fouled membranes (see Fig. 5). To evaluate the mean voxel amplitude on the feed side of the membrane system a binary mask was applied to the images to remove signal from permeate and perimeter stagnant water (see Fig. 5a). The mean pixel amplitude of the flowing region of the membrane was evaluated with and without the feed flow (Figs. 5b and 5c respectively). The decline of mean signal amplitude with increasing echo time for the no flow condition is due to T_2 relaxation of water molecules, with the fouled membrane having a significantly smaller mean signal amplitude when compared with the clean membrane, which indicates that the water in the fouled case has more rapid T_2 relaxation rate, which is consistent with previous results of alginate fouling in porous media [28]. The T_2 relaxation were independently measured to be 2.0 ± 0.1 s and 1.2 ± 0.1 s respectively for the stationary fluids inside the clean and fouled membrane systems, which accounts for the signal attenuation observed in Fig. 5b. For the flowing case (Fig. 5c) the effect of increased T_E is to substantially decrease the mean normalised signal amplitudes from approx. 7 to 2.5 due to the wash-out effect. At T_E= 200 ms

there is not much difference between the non-flowing (Q: 0 L/h) and flowing (200 L/h) scenarios *i.e.* 75% and 77% NMR signal retention for the clean and fouled membrane respectively. By comparison, at T_E = 800 ms the NMR signal retention between the non-flowing and flowing scenarios show a 33% vs. 43% NMR signal retention for the clean and fouled membrane respectively. The relative increase for the fouled membrane at the longer T_E is due to the effect of fouling, which causes fluid slow-down in some membrane regions leading to greater signal retention. To quantify this effect in terms of change in fluid residence time the following simplified expression shown in Fridjonsson et al. [29] is used to account for combined effects of T_2 relaxation and fluid wash-out on the normalised signal attenuation E:

$$E(t_E) = \frac{S_{t_E}}{S_0} = \left(1 - \frac{T_E}{\tau_d}\right)e^{-t_E/T_2} \tag{1}$$

where S_{t_E} is the normalised mean signal at time T_E, S_0 is the normalised mean signal at time $T_E = 0$, $\tau_d = L_d/U$ is the residence time in the detector and L_d is the effective length of the detector. Note that this makes the significant assumption of a single velocity and hence a single residence time – this is clearly not physically the case. By using T_2 values for the clean and fouled membrane at stationary conditions (Q: 0 L/h) it is possible to determine S_0 and to determine the change in fluid residence time for the clean and fouled membrane at Q: 200 L/h. By this analysis a 17% increase in mean fluid residence time accounts for the observed difference at T_E = 800 ms in Fig. 5c. This increase is indicative of the presence of some fluid that is essentially stagnant with a very large residence time. This confirms that significant alginate fouling has occurred in the membrane system due to the deviation from behavior characterized by a uniform residence time; this fouling is corroborated by the high field higher resolution images shown in Fig. 3.

In addition to the analysis of averaged signal amplitude effects, the fouled membrane images (*e.g.* Fig. 4d) shows "cloud-like"structure patterns when compared with the clean membrane images (*e.g.* Fig. 4b). The fouled membrane contains alginate gel trapped in the feed channel, which
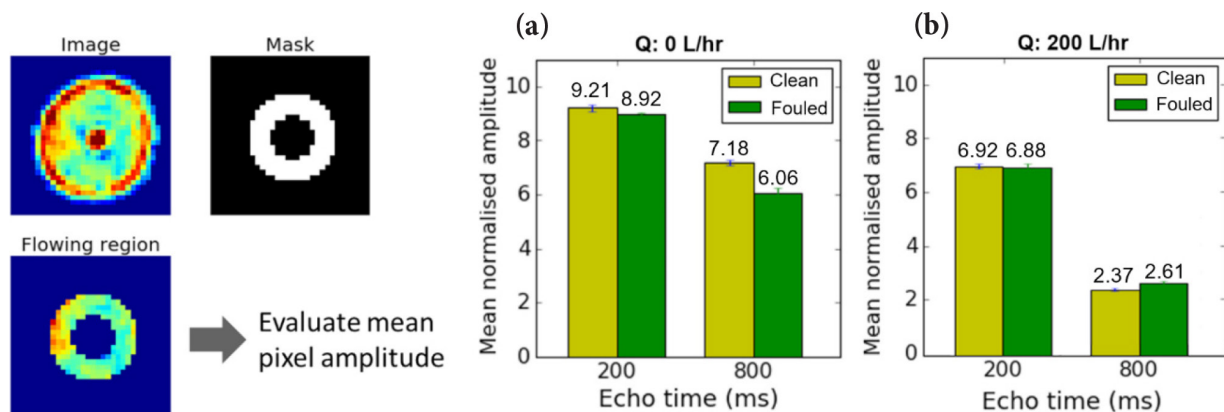

Fig. 5. Mean pixel amplitudes of the flowing region when the flow rate was (a) 0 L/h and (b) 200 L/h (error bar indicate 95% confidence interval based on the t-distribution). The loss in signal amplitude in (a) is due to T_2 relaxation, with a T_2 of 2.4 s for the clean membrane and T_2 of 1.6 s for the fouled membrane; The loss of signal amplitude in (b) is due to the combined effects of wash out and T_2 relaxation.

retains water and affects the fluid residence time distribution. The observed voxel pattern in the flowing region of the fouled membrane indicates that the signal is from water which is not washed away by cross-flow.

3.3. Statistical analysis on the similarity of the images

To further investigate the effect of fouling on the acquired images, changes in voxel signal intensity were compared between images acquired at different times and at different flowing and fouling conditions. This is an approach to identify if the structural effects seen in the images can differentiate clean and fouled membrane systems and therefore identify the location of fouling. The similarity of voxel patterns was evaluated by using Pearson's correlation [30]. The voxel-to-voxel correlation of the flowing region (the masked region as shown in Fig. 5a) was evaluated for images of the same echo time. High correlations (> 0.5) between the images of the same condition of the membrane (*e.g.* clean/clean and fouled/fouled) indicates good reproducibility of the measurement while the low correlations between the different conditions (clean/fouled) measures a dissimilarity of the two images. Fig. 6 shows a collage of MRI images acquired at each of the investigated conditions (clean/fouled) at T_E of 400 ms and 800 ms. Fig. 7 shows the comparison of the mean correlation values obtained from these images, with the standard deviation shown as error bars. The mean correlation value is obtained from at least 1482 correlation values from comparing every image pair (*e.g.* each clean membrane system image with each fouled membrane system image at T_E 400 ms). The results show that there is a high correlation (>0.6) between the images acquired with shorter echo times (in this

Clean Membrane (T_E: 400ms)

Clean Membrane (T_E: 800ms)

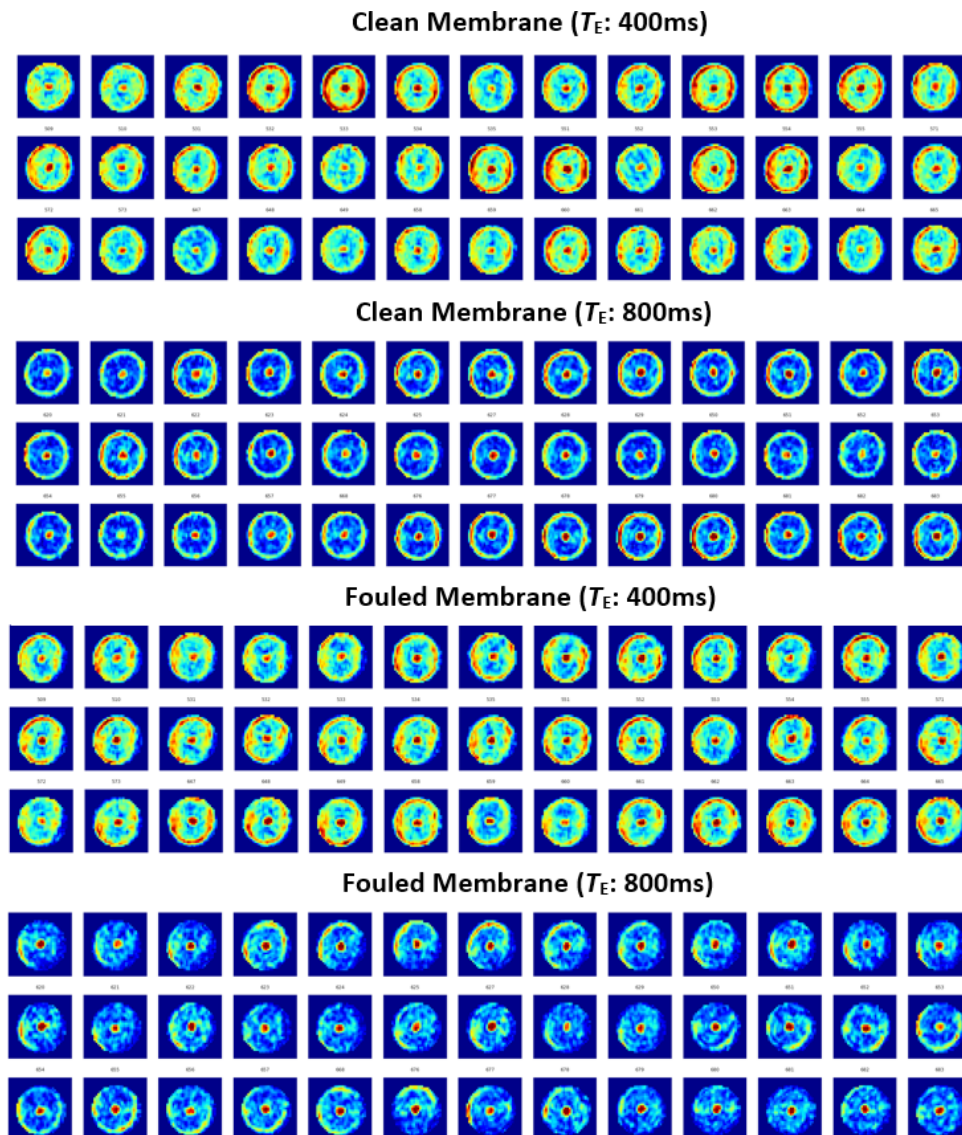**Fouled Membrane (T_E: 400ms)**

Fouled Membrane (T_E: 800ms)

Fig. 6. Shows a collage of MRI images obtained using the EF MRI for the clean and fouled membrane system at different echo times (T_E) of 400 ms and 800 ms. These images were statistically analysed to determine the similarity of images at different conditions (see Fig. 7) which showed that at T_E: 800 ms the clean and fouled membranes are structurally distinct.
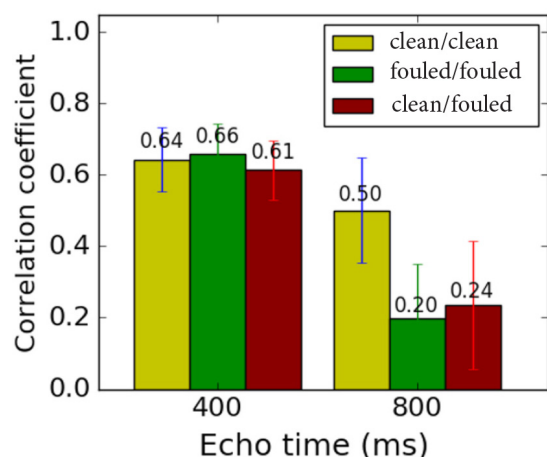
Fig. 7. Pearson's correlation coefficients evaluated between the clean/clean, fouled/fouled and clean/fouled membrane at different echo times (error bars indicate standard deviation), illustrating that an echo time of 800 ms enables discrimination between a clean and fouled membrane systems.

case T_E = 400 ms), which is comparable to values reported for other low signal-to-noise MRIs such as functional MRI [31], while the correlation between the images of the clean/fouled membrane is also high, indicating that the measurement did not differentiate the clean and fouled membrane at T_E of 400 ms. This is expected given the lack of signal contrast at shorter T_E conditions. For the images of echo time 800 ms there is a high correlation in the measurement of the clean membrane (0.50) while the fouled membrane shows a much lower correlation coefficient (0.20), indicating much higher variability with the fouled membrane. A comparison of the clean and fouled membrane (correlation coefficient 0.24) show that there is a distinct difference between the correlation values for the clean and fouled conditions at the higher echo time (T_E = 800 ms) indicating, that the LF-MRI is distinguishing between the fouled and clean membrane systems and therefore the LF-MRIs are indeed observing the structural effect of fouling in the images.

3.4. Implications of this research

In this study, alginate gel was introduced to the membrane to foul the feed side of a spiral wound reverse osmosis membrane system to intentionally foul the membrane and demonstrate the ability of LF-MRI to spatially detect the fouling. The study demonstrated that a low cost low magnetic field MRI instrument using relatively coarse image resolution can detect the difference between a clean and fouled membrane system.

The importance of being able to spatially locate fouling material inside a spiral wound geometry may allow the potential for *in-situ* monitoring of fouling inside commercial spiral-wound membrane systems. This expands upon the previously reported LF-NMR techniques [23] which monitored the effects of fouling without any imaging capability, *i.e.* ability to locate foulants in the radial direction. With the successful demonstration of the LF-MRI it is possible to develop specific low cost LF-MRI systems, *e.g.* NMR-

CUFF [32], for spiral wound modules that can be placed outside the existing pressure vessel allowing non-invasive spatial monitoring of fouling and the development of more effective cleaning strategies.

4. Conclusions

This work has shown the application of LF-MRI for the detection of fouling of a spiral-wound RO membrane system. The contrast between the flowing and stagnant water in the images can be controlled by adjusting the echo time of 2D spin-echo imaging pulse sequence. Fouling was detected by LF-MRI by evaluating the mean pixel amplitude of the flowing region of the membrane. In addition, the perceivable difference in the signal distribution pattern were statistically verified by evaluating Pearson's correlation coefficient. Showing that the LF-MRI technique can non-invasively spatially locate fouling inside membrane systems during operation. Further ongoing research is required to evaluate the sensitivity limit of LF-MRI for the earlier detection of membrane fouling. Future research will additionally look at the ability of the measurement technique to detect combined fouling (biological, organic and/or inorganic) and identify the fouling type. This study encourages further development of LF-MRI technology for the non-invasive monitoring and identification of fouling inside spiral wound membrane systems in operating commercial membrane installations.

References

[1] K.P. Lee, T.C. Arnot, D. Mattia, A review of reverse osmosis membrane materials for desalination—development to date and future potential, J. Membr. Sci., 370 (2011) 1–22.

[2] L.F. Greenlee, D.F. Lawler, B.D. Freeman, B. Marrot, P. Moulin, Reverse osmosis desalination: water sources, technology, and today's challenges, Water Res., 43 (2009) 2317–2348.

[3] A. Drews, C.-H. Lee, M. Kraume, Membrane fouling-a review on the role of EPS, Desalination, 200 (2006) 186–188.

[4] W. Guo, H.-H. Ngo, J. Li, A mini-review on membrane fouling, Bioresour. Technol., 122 (2012) 27–34.

[5] H.-C. Flemming, G. Schaule, T. Griebe, J. Schmitt, A. Tamachkiarowa, Biofouling—the Achilles heel of membrane processes, Desalination, 113 (1997) 215–225.

[6] S. Creber, J. Vrouwenvelder, M. Van Loosdrecht, M. Johns, Chemical cleaning of biofouling in reverse osmosis membranes evaluated using magnetic resonance imaging, J. Membr. Sci., 362 (2010) 202–210.

[7] J. Vrouwenvelder, M. Van Loosdrecht, J. Kruithof, Early warning of biofouling in spiral wound nanofiltration and reverse osmosis membranes, Desalination, 265 (2011) 206–212.

[8] H.-C. Flemming, T.R. Neu, D.J. Wozniak, The EPS matrix: the "house of biofilm cells", J. Bacteriol., 189 (2007) 7945–7947.

[9] J. Vrouwenvelder, J. Van Paassen, J. Kruithof, M. Van Loos-drecht, Sensitive pressure drop measurements of individual lead membrane elements for accurate early biofouling detection, J. Membr. Sci., 338 (2009) 92–99.

[10] J. Vrouwenvelder, S. Manolarakis, J. Van der Hoek, J. Van Paassen, W.G.J. van der Meer, J. Van Agtmaal, H. Prummel, J. Kruithof, M. Van Loosdrecht, Quantitative biofouling diagnosis in full scale nanofiltration and reverse osmosis installations, Water Res., 42 (2008) 4856–4868.

[11] G.-Y. Chai, A. Greenberg, W. Krantz, Ultrasound, gravimetric, and SEM studies of inorganic fouling in spiral-wound membrane modules, Desalination, 208 (2007) 277–293.

[12] E. Kujundzic, K. Cobry, A.R. Greenberg, M. Hernandez, Use of ultrasonic sensors for characterization of membrane fouling and cleaning, J. Eng. Fiber. Fabr., 3 (2008) 10.

[13] Y. Ye, P. Le Clech, V. Chen, A.G. Fane, B. Jefferson, Fouling mechanisms of alginate solutions as model extracellular polymeric substances, Desalination, 175 (2005) 7–20.

[14] P. van den Brink, A. Zwijnenburg, G. Smith, H. Temmink, M. van Loosdrecht, Effect of free calcium concentration and ionic strength on alginate fouling in cross-flow membrane filtration, J. Membr. Sci., 345 (2009) 207–216.

[15] N. Farhat, M. Staal, A. Siddiqui, S. Borisov, S.S. Bucs, J.S. Vrouwenvelder, Early non-destructive biofouling detection and spatial distribution: application of oxygen sensing optodes, Water Res., 83 (2015) 10–20.

[16] J. Kavanagh, S. Hussain, T. Chilcott, H. Coster, Fouling of reverse osmosis membranes using electrical impedance spectroscopy: measurements and simulations, Desalination, 236 (2009) 187–193.

[17] L. Sim, Z. Wang, J. Gu, H. Coster, A. Fane, Detection of reverse osmosis membrane fouling with silica, bovine serum albumin and their mixture using in-situ electrical impedance spectroscopy, J. Membr. Sci., 443 (2013) 45–53.

[18] S.-T. Kang, A. Subramani, E.M. Hoek, M.A. Deshusses, M.R. Matsumoto, Direct observation of biofouling in cross-flow microfiltration: mechanisms of deposition and release, J. Membr. Sci., 244 (2004) 151–165.

[19] C. Dreszer, A.D. Wexler, S. Drusová, T. Overdijk, A. Zwijnenburg, H.-C. Flemming, J.C. Kruithof, J.S. Vrouwenvelder, In-situ biofilm characterization in membrane systems using Optical coherence tomography: formation, structure, detachment and impact of flux change, Water Res., 67 (2014) 243–254.

[20] R.C. Chen, Q. Li, M. Elimelech, In situ monitoring techniques for concentration polarization and fouling phenomena in membrane filtration, Adv. Colloid. Int. Sci., 107 (2004) 83–108.

[21] R. Valladares Linares, L. Fortunato, N.M. Farhat, S.S. Bucs, M. Staal, E.O. Fridjonsson, M.L. Johns, J.S. Vrouwenvelder, T.O. Leiknes, Mini-review: novel non-destructive *in situ* biofilm characterization techniques in membrane systems, Desal. Water Treat., 57 (2016) 22894–22901.

[22] L.N. Sim, T.H. Chong, A.H. Taheri, S.T. Sim, L. Lai, W.B. Krantz, A.G. Fane, A review of fouling indices and monitoring techniques for reverse osmosis, Desalination, 434 (2018) 169–188.

[23] E. Fridjonsson, S. Vogt, J.S. Vrouwenvelder, M. Johns, Early non-destructive biofouling detection in spiral wound RO membranes using a mobile earth's field NMR, J. Membr. Sci., 489 (2015) 227–236.

[24] E.O. Fridjonsson, S.A. Creber, J.S. Vrouwenvelder, M.L. Johns, Magnetic resonance signal moment determination using the Earth's magnetic field, J. Magn. Reson., 252 (2015) 145–150.

[25] M.E. Halse, A. Coy, R. Dykstra, C. Eccles, M. Hunter, R. Ward, P.T. Callaghan, A practical and flexible implementation of 3D MRI in the Earth's magnetic field, J. Magn. Reson., 182 (2006) 75–83.

[26] L. Axel, Blood flow effects in magnetic resonance imaging, AJR Am. J. Roentgenol., 143 (1984) 1157–1166.

[27] D.G. Von Der Schulenburg, J. Vrouwenvelder, S. Creber, M. Van Loosdrecht, M. Johns, Nuclear magnetic resonance microscopy studies of membrane biofouling, J. Membr. Sci., 323 (2008) 37–44.

[28] H.T. Fabich, S.J. Vogt, M.L. Sherick, J.D. Seymour, J.R. Brown, M.J. Franklin, S.L. Codd, Microbial and algal alginate gelation characterized by magnetic resonance, J. Biotechnol., 161 (2012) 320–327.

[29] E.O. Fridjonsson, P.L. Stanwix, M.L. Johns, Earth's field NMR flow meter: Preliminary quantitative measurements, J. Magn. Reson., 245 (2014) 110–115.

[30] D.C. Montgomery, G.C. Runger, Applied statistics and probability for engineers, John Wiley & Sons, 2010.

[31] K. Wagner, L. Frings, A. Quiske, J. Unterrainer, R. Schwarzwald, J. Spreer, U. Halsband, A. Schulze-Bonhage, The reliability of fMRI activations in the medial temporal lobes in a verbal episodic memory task, Neuroimage., 28 (2005) 122–131.

[32] C.W. Windt, H. Soltner, D. Van Dusschoten, P. Blümler, A portable Halbach magnet that can be opened and closed without force: the NMR-CUFF, J. Magn. Reson., 208 (2011) 27–33.